Universiteit
Leiden
The Netherlands

Automatic quantification of intravascular optical coherence tomography

Wang, A.

Citation
Wang, A. (2014, November 13). *Automatic quantification of intravascular optical coherence tomography*. Retrieved from https://hdl.handle.net/1887/29690

Version:	Corrected Publisher's Version
License:	Licence agreement concerning inclusion of doctoral thesis in the Institutional Repository of the University of Leiden
Downloaded from:	https://hdl.handle.net/1887/29690

Note: To cite this publication please use the final published version (if applicable).

Cover Page

Universiteit Leiden

The handle http://hdl.handle.net/1887/29690 holds various files of this Leiden University dissertation

Author: Wang, Ancong
Title: Automatic quantification of intravascular optical coherence tomography
Issue Date: 2014-11-13

CHAPTER

1

Introduction and outline

1.1 Cardiovascular system

The cardiovascular system is a blood distribution network which consists of the heart, blood vessels, and blood. The heart is about the size of a closed fist and functions as the body's circulatory pump which takes in deoxygenated blood returned from the body and delivers it to the lungs to release carbon dioxide and absorb oxygen before pumping it into the artery network. On average, the heart beats 70 times per minute and even at rest, the heart can easily pump over 7 ton of blood throughout the body every day. Blood vessels transport blood from the heart to all body tissue and back again quickly and efficiently. There are three major types of blood vessels: the arteries, which carry blood away from the heart; the capillaries, where the actual exchange of gases, nutrients, and waste products between the blood and the tissues takes place; and the veins, which carry blood back to the heart. All vessels contain a hollow area called the lumen through which blood can flow and the lumen size corresponds with the amount of blood that can pass through it. Blood is composed of blood cells suspended in plasma. On average, an adult has about 5 liters of blood. The main function of blood is to deliver substances like nutrients, wastes, hormones and gases which not only help to maintain the body's homeostasis, but also play major roles in the body's defense against infection [1, 2].

1.2 Coronary circulation

The heart powers the whole cardiovascular system [3] while the blood transported to the myocardium is delivered by the coronary circulation in which the left and right coronary arteries branch off from the aorta and deliver oxygen-rich blood to the left and right sides of the heart. The deoxygenated blood from the heart muscle is returned to the vena cava by the coronary sinus. Figure 1 shows part of the cardiovascular system near the heart including the coronary circulation system. Only when healthy, these arteries are capable of autoregulation to maintain coronary blood flow at levels that appropriate to the heart muscle demands. Since the coronary circulation is the only source of blood supply to the myocardium and it contains little redundant blood supply, the ischemia caused by coronary vessel narrowing or blockage could be fatal [4].

1.3 Coronary artery disease

Coronary artery disease (CAD), which causes coronary heart disease (CHD), is the number one cause of death in the developed countries and a major cardiovascular disease in the rest of the world. Healthy arteries are elastic and smooth, but when CAD occurs, mixtures of cholesterol, inflammatory cells, lipoprotein and calcium, called plaques, start to deposit under the intima. The artery walls become thick and rigid while plaques release chemicals to promote the healing. In addition, plaques slowly build up and narrow the coronary arteries so that the blood flow to the myocardium becomes insufficient as Figure 2 presented. On the other hand, the ischemia can occur acutely as a sudden rupture of vulnerable plaques or thrombi can immediately reduce or even totally block the blood supply to heart or other organs. The traditional risk factors for CAD are high level of low-density lipoprotein (LDL) cholesterol, low level of high-density lipoprotein (HDL) cholesterol, high blood pressure, family history, diabetes, smoking, being older than 55 for women and being older than 45 for men.

High stress, lack of physical activity and obesity are also suspicious risk factors [5]. Without proper treatment, CAD will weaken the heart muscle and lead to arrhythmias, heart attack, heart failure and stroke.

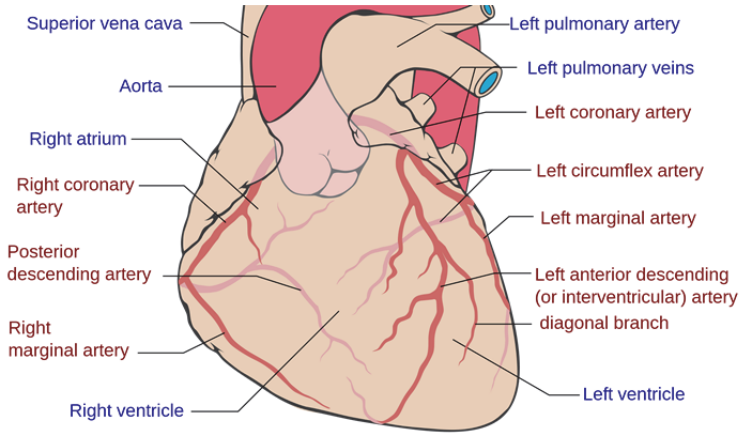

Figure 1-1. Part of the cardiovascular system near the heart including four heart chambers, main arteries and veins are labelled in blue text. On the heart, the coronary vessels are labelled in red text. (Source: http://en.Wikipedia.org/wiki/ File:Coronary_ arteries.png)

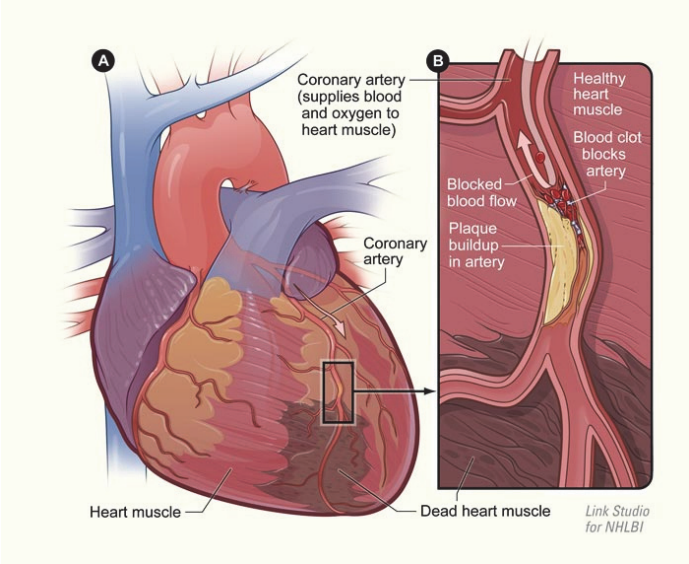

Figure 1-2. Coronary artery disease is caused by plaques build up in the coronary artery. Plaques can rupture and cause blood clots which block the supply of blood and oxygen to the heart. A blockage that is not treated properly will cause the affected heart muscle to die. (Source: http://www.nlm.nih.gov/medlineplus/ magazine/issues/ winter09/articles/winter09pg25-27.html)

1.4 CAD treatment

CAD cannot be fully cured, but in most of the cases, proper treatments are able to relieve the symptoms like chest pain and lower the risk of death. There are three main strategies of treatment: lifestyle changes, medications and medical interventions.

A healthy lifestyle including weight control, smoking cessation, physical exercise and healthy diet can be a preventive measure to delay or even prevent the atherosclerosis development which usually takes many years and could have no sign at all in the beginning. Patients with CAD can also benefit from the healthy lifestyle as it reduces the risk of further episodes and there is hope that CAD can be regressed before it causes serious CHD.

When lifestyle changes are insufficient, many different types of medications can be used to treat CAD. Antiplatelet drugs, such as aspirin, can keep platelets in the blood from sticking together. Anticoagulants are another class of drugs that prevent blood from clotting. Cholesterol-modifying drugs, like statins, decrease the level of LDL cholesterol which is one of the primary materials of plaques. Calcium channel blockers are used to decrease blood pressure, alter heart rate and alleviate chest pain. Beta blockers can reduce the oxygen request of myocardium by lowering the heart rate and blood pressure. On the other hand, Nitroglycerin can relax coronary arteries to increase the blood supply. Medications may help patients to delay or even avoid the demands of medical surgery. However, medications usually have side effects and are limited when facing severe CAD situations.

Medical interventions are required when lifestyle changes and medications do not work sufficiently. Coronary surgery and percutaneous coronary intervention (PCI) are the two primary means of revascularization. Coronary artery bypass graft (CABG) surgery was first introduced in 1960 and the idea is grafting healthy arteries or veins from other parts of the body to the narrowed coronary arteries. The grafted vessel bypasses atherosclerotic narrowing and creates a new path for blood flow to the heart muscle. CABG is particularly suitable for situations like the left main coronary artery blockage, multiple artery narrowings and poor heart function, but also has risks as any type of surgery.

PCI is a class of nonsurgical procedures that utilize coronary catheterization to open narrowed or even blocked coronary arteries, which serves as a chance for non-surgical candidates [6]. Coronary catheterization accesses the coronary circulation and blood filled chambers of the heart using a catheter for both diagnostic and interventional (treatment) purposes. During the catheterization, a guide wire is inserted into a big vessel in the arm or groin through a needle, and threaded to the heart under the guidance of a special x-ray imaging system. It helps doctor position catheters correctly. Next, the needle is replaced by a tapered tube called sheath. Through the sheath, a hollow guiding catheter is slid over the guide wire to the target region and then the guide wire can be removed. After the catheter reaches the right spot, diagnostic tests or treatments on the heart can be applied through it. For PCI treatment, a second guide wire is threaded through the guide catheter and passes the vessel blockage. It assists another catheter with a balloon on the end (balloon catheter) through the guide catheter to the narrowed region. Once in place, the balloon is inflated with a high pressure to push the plaque against the artery wall, relieving the blockage and restoring blood flow. Next, the balloon is deflated and withdrawn together with the catheter, guide wire and sheath. Unless the artery is too small, a

medical device called stent can be implanted during the PCI. A coronary stent is a tiny tube-like mesh that is used to support the narrowed vessel wall and keep the lumen open during the follow up. When implanting, a stent is constrained on a deflated balloon and delivered to the narrowed region during or after the balloon angioplasty. While the balloon is expanding, the stent is opened to support the vessel wall (Figure 3). In addition, there are also self-expanding stents. An introduction of stent is given in the next section. The advantages of PCI relative to CABG include less procedure time, ease of use, no general anesthesia, faster patient recovery and decreased systemic complications. Commonly, PCI is the first choice for stable as well as unstable CAD patients and it may delay or eliminate the future need for coronary artery bypass surgery [7-9].

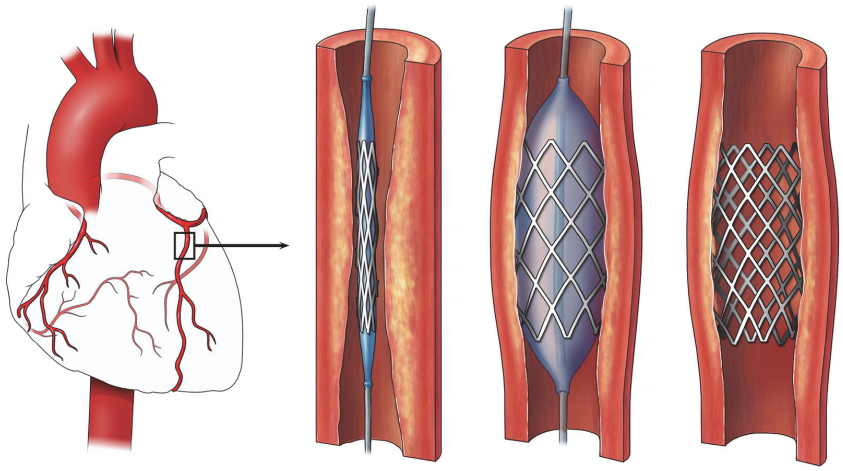

Figure 1-3. Stenting for coronary artery disease. First, the stent restricted on a deflated balloon is threaded to the narrowing of the vessel. The balloon is inflated to press plaques against the vessel wall and open the stent at the same time. The balloon is deflated and removed, leaving the stent to keep the lumen open. (Source: http://www.themedschoolproject.com/2012/02/valentines-day-special-way-to-mans.html)

1.5 Coronary stent

1.5.1 Bare metal stents

The PCI procedure, which was pioneered by Grüntzig in 1977, has become the most frequently performed therapeutic procedure in medicine [10]. The coronary balloon angioplasty was a breakthrough in treating CAD and quickly accepted worldwide. However, unpredictable risks of acute vessel closure caused by occlusive coronary dissection became evident. Sometimes, an emergency CABG surgery is required to save the patient. Besides, in up to one third of cases, too much tissue grows within the treated portion of the artery which re-narrows or even blocks the artery during the follow-up [11]. It is called late restenosis and mainly caused by constrictive remodeling [12, 13], elastic recoil [14] or the neointimal hyperplastic healing response [14, 15]. Although the luminal enlargement could be performed many times, it costs

more and does not eliminate the risks. These problems diminished the value of balloon angioplasty.

After a series of trial tests [16, 17], bare metal stents (BMS) were heralded as the second revolution in interventional cardiology to overcome the disadvantages of balloon angioplasty [11]. It provides a solution to acute vessel closure by moving intimal and medial flaps away from the lumen and maintaining radial support to prevent elastic recoil. The rate of sub-acute occlusion was successfully reduced to 1.5% so that emergency bypass surgery becomes a rare occurrence during the PCI. Furthermore, the late restenosis rate was significantly decreased by more than 10% [17]. By 1999, angioplasty paired with coronary stent implantation comprised 84.2% of all PCI procedures [18].

1.5.2 Drug-eluting stent

Despite the tremendous success in preventing the acute recoil and post-injury arterial shrinkage associated with balloon angioplasty, BMS still has a high restenosis rate of 22% during the follow up. As the implanted stents are foreign objects, they increase the risk of sub-acute thrombosis and late in-stent neointimal hyperplasia. The neointimal hyperplasia inside the stent was even more prominent than with balloon angioplasty, necessitating repeat treatment in numerous patients [19].

To reduce the in-stent neointimal hyperplasia, drug-eluting stents (DES) were invented. A drug-eluting stent consists of three components: a metallic stent as the platform, a polymer layer covering the stent as the carrier and some antiproliferative medicines as the agent. The medicines are slowly and continuously released into the artery to prevent it from becoming blocked again. Large trials have proved that the in-stent restenosis rate dropped greatly, but the increased risk of late stent malapposition and late stent thrombosis became evident [10].

1.5.3 Bioresorbable vascular scaffold

Metallic stents, including BMS and DES, are both permanent devices. As they caged the vessel, late luminal enlargement and advanced vascular remodeling could no longer occur. To solve their problems, the principle of temporary vascular scaffold, called bioresorbable vascular scaffold (BVS) was put forward (Figure 4). A BVS should provide a solid support to the vessel wall after the implantation to prevent acute vessel closure and recoil and persistently release antiproliferative medicines to prevent the restenosis. After restoring the artery, the scaffold will be fully degraded or resorbed during the follow-up. In the end, a BVS leaves no foreign object in the vessel but all future options open for the patient. Current trials showed that BVS has a better outcome in many fields than metallic stents [20, 21]. This nascent technology is evolving rapidly and more research and trials are ongoing for validation and improvement.

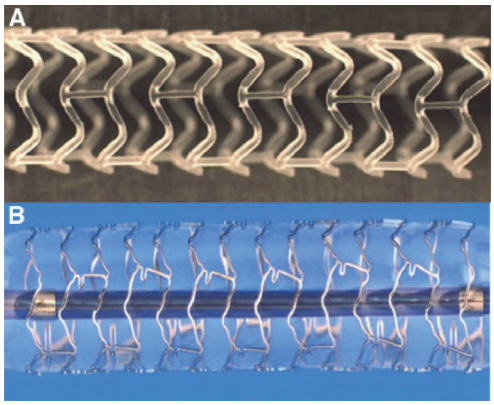

Figure 1-4. A comparison of a bioresorbable vascular scaffold (A) and a drug-eluting stent (B) (Source: http://interventions.onlinejacc.org/article.aspx?articleid= 1112042)

1.5.4 Stent design

Over the years, stent designs including pattern, material, coating and tissue-metal interface have been developed in addition to accompanying drug treatments. Although none of the current designs of coronary stents are ideal, constant research and improvement are being made especially with respect to homogeneous distribution of force, ease of placement, stability and conformability [22]. For example, the stent cell pattern affects the ability of vessel wall support. Small cells usually have better support but they can lower the side branch access through them.

1.6 Invasive imaging techniques

Symptoms of CAD, like chest pain, shortness of breath, palpitations and even fatigue, can be used for diagnosis. However, to diagnose and evaluate the CAD accurately, medical imaging techniques are necessary. For the past fifty years, sophisticated research of imaging the heart and vascular vessels has been studied enormously. Two main strategies of imaging techniques have been investigated: invasive imaging, such as coronary angiography, intravascular ultrasound (IVUS) and intravascular optical coherence tomography (IVOCT) and noninvasive imaging, such as computed tomography (CT), magnetic resonance imaging (MRI), x-ray and echocardiography. In the beginning, noninvasive methods were most preferred as they are safe and cheap. After the increased understanding of coronary artery diseases, the limitation of noninvasive methods became evident as they do not have sufficient resolution and penetration to give a detailed description of small structures, for example atherosclerosis, specifically vulnerable plaque with thin cap, the neointimal thickness and tissue coverage of struts. Nowadays, invasive imaging methods have become dominant for CAD diagnosis and treatment guidance.

1.6.1 Coronary angiography

Coronary angiography, since the 1960s, has been one of the most matured invasive imaging techniques for artery blockage diagnosis, evaluation and treatment. It is a modality that utilizes special x-ray and harmless dye (contrast) to show the insides of arteries. Similar as the PCI procedures, it is applied using the cardiac catheterization

procedure. Once the catheter is properly placed, the contrast will be injected through the catheter and released into the bloodstream. The mixture flows through the coronary arteries, making the lumen visible in the x-ray images. Due to the volume of the mixture, the vessel lumen size can be appreciated so that when a plaque has built-up inside an artery, a narrowed or restricted blood flow can be visualized. If the angiography reveals a blocked artery, a PCI procedure could be applied to restore blood flow instantly and the contrast will be injected again to assess the treatment outcome.

Coronary angiography is the traditional way of imaging during diagnostic and interventional coronary procedures as it can easily provide an accurate real-time illustration. The images can support accurate and highly reproducible measurements for clinical decision-making and research to estimate the regression and progression of coronary obstructions, particularly the lumen size, for the PCI outcome assessment [23]. However, coronary angiography loses accuracy in the presence of vessel superposition or foreshortening. Furthermore, only the lumen of the vessel is visualized by x-ray angiography, while the information about the vessel wall and plaque is absent. Therefore, it only has limited ability to characterize tissue and plaques beyond the detection of dissections and very advanced plaques with extensive calcification in the vessel wall. Thus, there are some scenarios in which complementary information is required besides the coronary angiography.

1.6.2 IVUS

IVUS imaging is a sound-based technique for visualizing arterial structure. A catheter with a high frequency ultrasound transducer mounted on the tip is threaded to the target vessel region by using cardiac catheterization. Because circulating blood is an excellent medium for transmission of ultrasound waves, the ultrasound transducer can emit a beam of ultrasound to the vessel tissue and receive the echo signal to acquire two-dimensional (2D) cross-sectional images of coronary arteries. The catheter is pulled back through the target region to generate real-time three-dimensional (3D) images and the images are recorded on the fast external storage for future analysis.

The frequency of ultrasound used in IVUS has a typical range of 20 - 40 MHz. The higher frequency of the signal results in the higher resolution of the images, but the lower penetration depth of tissue. Current IVUS imaging systems have a resolution of 100 – 250 μm. IVUS not only has the advantage of accurate determination of luminal dimensions of vessels, but also has the potential to assess the presence and extent of the atherosclerotic plaque and the characterization of arterial wall components. Compared with coronary angiography, IVUS does not cause radiation damage or require contrast injection. However, its common pullback speed is only 0.5 - 1 mm/sec, therefore, the IVUS imaging can be influenced by cardiac motion. Furthermore, the IVUS resolution still has limitations when measuring tiny structures like the vulnerable cap of a plaque.

1.6.3 IVOCT

IVOCT has emerged as an attractive new imaging modality, which offers superior resolution (approximately 10 μm) for in-vivo coronary plaque morphology. Figure 5(A) illustrates a commercial IVOCT system. Like IVUS, IVOCT uses an imaging catheter to acquire cross-sectional images of the target vessel, but instead of ultrasound, the

IVOCT imaging catheter emits near-infrared light beam to the vessel tissue. Due to the speed of light, interferometry techniques are necessary to measure the backscattered light since a direct quantification is not available. The reflected light from a point of the sample and the reference light generate an interference pattern so that a detector can create a pixel for this specific site based on the produced light and dark pattern. The imaging catheter is being rotated and pulled back by a motor when acquiring images and a fluid-filled semitransparent polymer tube, named protective sheath, is used to cover the imaging catheter. After scanning cross-sections successively at different transverse positions, a full 3D image of the vessel is generated. This procedure is usually assisted by a standard guide wire. Therefore, a typical IVOCT image always contains the imaging catheter, protective sheath, guide wire and vessel lumen. Besides these common components, there also could be stent struts, side branches, thrombi, plaques and other lesions. The major limitation of IVOCT is blood attenuation due to the backscattering properties of red blood cells, thus the blood is temporarily displaced from the field of view during imaging acquisition by infusing saline or contrast through the vessel. An example of a typical IVOCT image is given in Figure 5(B).

There are two IVOCT imaging systems: the time-domain IVOCT and the frequency-domain IVOCT [24]. The frequency-domain IVOCT imaging system facilitates high-speed pullbacks (20 mm/sec) during image acquisition without necessitating transient balloon occlusion of the coronary artery. The high pullback speed also greatly alleviates the impact of cardiac motion. However, some errors and artifacts still can be found in IVOCT images which may induce imprecise assessment and measurements. For example, the optic path length of the imaging catheter could be slightly different during the whole pullback run which results in different image scale as Figure 5(C) presented. Hence, an image calibration, called Z-offset correction, should be applied throughout the entire pullback to adjust the image scale. If the blood is not completely displaced, there will be residual blood in the lumen which blurs the boundary of the protective sheath and lumen like Figure 5(D). Residual blood artifacts also could be mistakenly labelled as thrombi. The small air bubbles inside the protective sheath can cause bright noise which will significantly attenuate the signal from behind and make poor definition of the protective sheath and imaging catheter. The seaming artifact is the result of rapid artery or imaging catheter shifting in a single frame, leading to misalignment of the lumen border. Figure 5(E) illustrated these two artifacts. In addition, when the imaging catheter passes a vessel tortuosity or simply sweeps during the pullback, its rotational speed could be nonuniform which conduces to nonuniform rotational distortion. It would lead to shape distortion or focal image loss [24-27]. There are also artifacts owing to the eccentric catheter position, such as sunflower artifact of metallic stent struts which appears as a bending of stent struts toward the imaging catheter. It means that a metallic strut parallel to the lumen wall could appear obliquely oriented to the lumen wall because when the light beam from the imaging catheter rotates over the strut, only the portion that is perpendicular to the light beam reflects light back. Thus, the strut orientation and apposition could be mistakenly assessed [28, 29]. An example is given in Figure 5(D). All these artifacts should be reduced in the next-generation IVOCT systems.

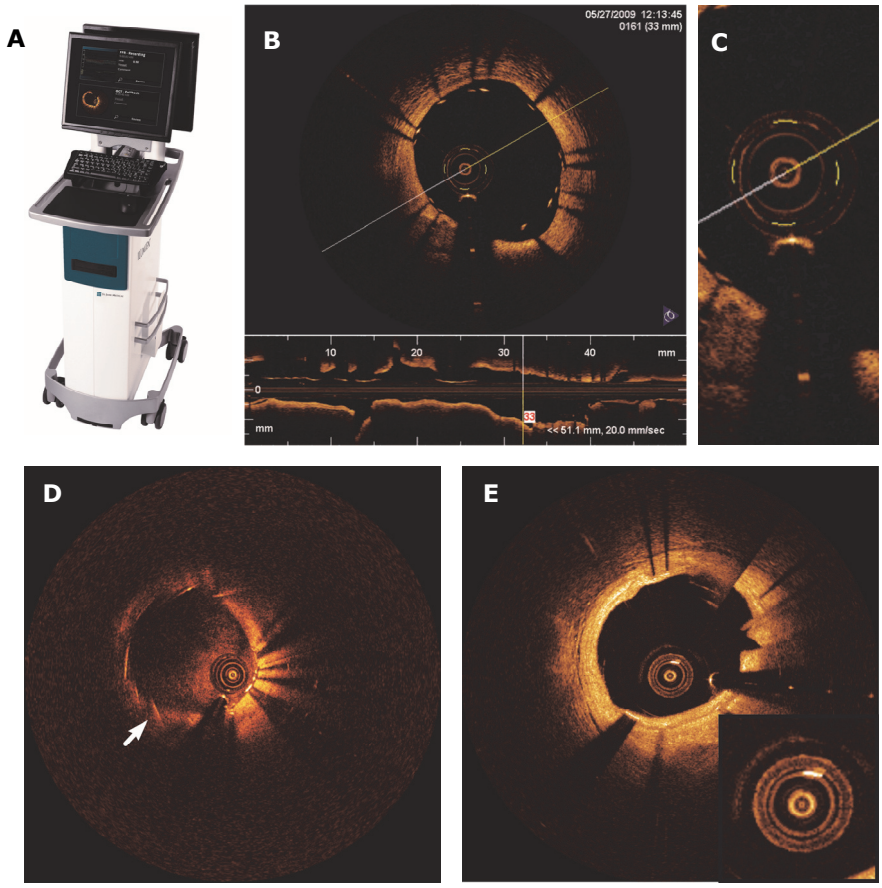

Figure 1-5. An IVOCT imaging system (St. Jude Medical, Westford, MA, USA) and an IVOCT image are presented in the figures (A) and (B). The top part of (B) is the cross-sectional image of vessel lumen which including the imaging catheter, protective sheath, guide wire, vessel lumen and metallic stent struts. The bottom section illustrates the longitudinal cut-up view of the whole scanned vessel region. The image center region is zoomed in in figure (C) which indicates the Z-offset correction failure as the 4 fiduciaries should align to fit the outer surface of the protective sheath. In figure (D), the residual blood results in bright noise inside the lumen and the eccentric imaging catheter causes the sunflower artifact of metallic stent struts (Arrow). An example of bubble noise in the protective sheath is given in figure (E) at 1 o'clock and the image behind it is blurred relative to other regions. At 2 o'clock, there is also a seaming artifact. (Source: http://professional-intl.sjm.com/products/vas/intravascular-diagnostics-imaging/ffr-oct/c7-xr-oct-intravascular-imaging-system#overview)

Although not perfect, IVOCT is currently the only intravascular imaging technique having sufficient resolution to delineate the microscopic characteristics of fine structures, such as the thin fibrous cap thickness, thin neointimal hyperplasia and plaque type. Moreover, IVOCT can detect subtle structural changes after PCI procedures, such as plaque disruption including tissue prolapse and protrusion with

high sensitivity [30]. Due to the high frequency light source, IVOCT has a limited penetration ability of about 3 mm. However, within the limitation, IVOCT has better sensitivity and specificity for detecting calcification, lipid pool, fibrous cap, fibrosis, neointimal hyperplasia, intracoronary thrombus and thin cap plaque than IVUS [31]. IVOCT has been increasingly used for PCI guiding and evaluation [32].

1.7 Image processing challenges in IVOCT images

In recent years, IVOCT with both original 2D cross-sectional images and 3D reconstructions has been a powerful tool in the diagnosis and treatment of complex CAD. The demand for IVOCT-based applications is increasing, such as IVOCT-guided PCI, stent analysis and diagnostic assessment of coronary atherosclerosis including lipid necrotic core, thin fibrous cap, and inflammation region. Althougth enormous progress has been made since the invention of IVOCT, there are still increasing challenges in IVOCT image processing. The imaging catheter, guide wire, protective sheath and lumen are the common components in all typical IVOCT pullback runs and need to be segmented in many situations. For example, because the high intensity of imaging catheter affects the lumen segmentation, S. Tsantis, et al. detected the imaging catheter using Hough transform [33]. However, this method could be influenced by imaging catheter mirror artifacts [34] which appear as several concentric circles around the real imaging catheter. In order to measure in-stent neointimal hyperplasia, S. Gurmeric, et al. removed the imaging catheter by using a Gaussian filter and a morphological opening operation [35], which erases many details from the image and does not result in the position of imaging catheter. We also found that the imaging catheter can also mislead stent strut detection which is based on intensity analysis and it can be segmented by applying a min-filter over the whole pullback run in the z-direction [36]. However, this method is only applicable to Z-offset corrected pullback runs in which the imaging catheter is located in the same position. Appearing like a metallic stent strut, a guide wire could be mistakenly detected as a strut by many methods [36-39] and should be filtered out. Moreover, the guide wire and its shadow can obstruct the protective sheath and lumen contour detection, vessel wall analysis and 3D reconstructions [40, 41]. In the current commercial IVOCT systems, the protective sheath acts as a reference for optimal Z-offset determination within a pullback run because it has a fixed diameter [26]. This calibration of Z-offset is critical for accurate measures as 1% change in the magnitude of the ideal Z-offset can result in about 13% error in area measurements. Besides, small Z-offset errors can also amplify contour distortion, which may result in misinterpretation of the image [25]. However, the current calibration can fail due to the air bubble noise in the protective sheath, wrong manual adjustment and proximity of protective sheath to vessel wall. According to statistics, only 38% of the IVOCT images illustrated in peer-reviewed papers were calibrated correctly [34]. Lumen contour detection is one of most common image segmentation steps for such as region of interest definition, in-stent restenosis and lumen area measurement. The existing methods include Markov random field and wavelet transform analysis [33], fuzzy c-means clustering and wavelet transform [42] or deformable spline model [35]. However, in many cases, a light-weight and fast lumen contour estimation is more suitable for real-time applications.

IVOCT images have already been extensively used to guide, analyze and evaluate the stent implantation, which leads to optimized stent size, inflation pressure, deployment position and post-processing which thereby reduces the risk of restenosis

and thrombosis and increases the post-intervention minimal stent area. For example, an under-expanded stent cannot provide sufficient support to the vessel wall and thereby can result in late neointimal hyperplasia. Before covered by healing tissue, malapposed struts are also a main predisposing factor of acute in-stent thrombosis. Accurate strut position detection in the post-stenting IVOCT images can verify stent apposition to the vessel wall and provide additional information related to the presence of edge dissections, stent fracture, plaque protrusion, and the need for post-dilation or additional stenting. Detected struts also assist the 2D strut distribution analysis because nonuniform struts can influence the stenting treatment outcome. Fewer struts and a big maximum inter-strut angle contribute to in-stent restenosis, plaque rupture and thrombus [43-45]. The demands of 3D stent reconstruction have been rising as it is a more effective way to present the deployed stents and offers the possibilities for precise stent measurements, such as stent cell size and maximum circular unsupported area. Furthermore, 3D stent cell pattern can affect the spatial support to the vessel wall, bending flexibility and the dosing of antiproliferative medicines released from DES. Hence, both 2D and 3D information are necessary for stent design evaluation and optimization [46-49]. In addition, the strut area is of interest for the analysis of the bioresorption process of neoteric bioresorbable vascular scaffolds [50, 51].

Side branch detection is another important application as they are one of the most reliable landmarks for image registration and labeling. In both research and clinical practice, features in IVOCT pullback runs at different time-points may need to be compared, for instance, the valid lumen size or BVS strut area. IVOCT is also popular in image fusion with many other modalities like IVUS and near-infrared spectroscopy images, which would offer more tissue characterization information to increase our understanding of vessel morphology and aid the management of complex vascular pathology. Besides, the position and size of side branches in the lesion region should be taken into account for stenting and blood volume analysis as a stent in front of a side branch can cause thrombus formation and obstruct the blood flow to the side branch. With both 3D reconstructed stents and side branches, cardiologists can assess the side branch access through stent cells, which may help them to decide if the stent ostium in front of a side branch needs to be expanded [52-55].

1.8 Motivation and objectives

As mentioned above, IVOCT, as a novel imaging modality, has played an active role in a wide range of CAD applications, including research and clinical routine. Due to its unparalleled high resolution and the ability to delineate complex vascular structures [56], IVOCT technology makes many precise measurement and novel applications possible. However, currently, a lot of analyses in IVOCT images are still relying on the manual work which decreases their value. The goal of this thesis is to develop robust and accurate (semi)automated methods that can detect and segment the interesting components in IVOCT pullback runs, such as implanted stent struts and side branches in 3D for accurate measurement, so that the results could contribute to medical research as well as for clinical decision-making. As such, the specific objectives of this thesis are threefold:

1. To develop fast and reproducible approaches for the metallic stent strut and BVS strut detection in IVOCT pullback runs for quantitative analysis, 3D reconstruction and PCI improvement.

2. To precisely measure the stent cell size and side branch access through stent cells in 3D space by reconstruct stent cell contours and stent surfaces based on the detected struts, so that the stent influence to the vessel wall and side branches could be assessed.

3. To detect side branches in IVOCT pullback runs fully automatically based on precise segmentation of all the common components in typical IVOCT images for stenting optimization and image registration. The segmentation methods also can be used for other advanced image processing.

1.9 Thesis outline

The remainder of this thesis is organized as follows:

Chapter 2 presents a novel automated algorithm to detect metallic stent struts in IVOCT pullback runs [57]. This method detects the pixels that belong to a strut by analyzing the intensity profile of every scan line and clusters these pixels using the constraint of stent strut shadow regions. Guide wires are automatically removed. The detected struts can later be used for 3D stent reconstruction, coverage measurement, implantation validation and follow-up analysis.

Chapter 3 introduces an automatic method to detect the new BVS struts in IVOCT pullback runs [58]. The translucency BVS struts appear as black cores with bright boundaries which are very different from the metallic stent strut. Two different strategies were used for BVS strut detection in baseline and follow-up datasets, separately. In both situations, the black core areas are segmented and their centers are computed. The validation results suggest that this method can be a useful tool for BVS analysis and 3D visualization.

Chapter 4 studies the impact of an implanted stent to the vessel wall and side branches in the deployment region [52]. Stent cells are reconstructed in 3D space through simple user interactions in 2D space. Stent cell size is measured based on a precisely reconstructed 3D stent surface from detected struts. Moreover, a 2D approximation of the 3D stent cell surface is generated for maximum circular unsupported surface area measurement. In the end, stent covered side branches are segmented to combine with stent cells for side branch access measurement. The accuracy and robustness of this method were validated in both phantom and in-vivo IVOCT datasets.

Chapter 5 describes a fully automated side branch detection method which utilizes a precise segmentation pipeline for all the common components in typical IVOCT pullback runs including imaging catheter, guide wire, protective sheath and lumen [59]. The algorithmic results from segmentation pipeline and side branch detection method contain only a little error compared with the ground truth and, thereby suggest the new segmentation and detection methods could be used to improve our previous presented methods, guide stenting operation and register images.

Chapter 6 summarizes the main work described in different chapters of this thesis. This chapter also includes the future perspectives on the IVOCT imaging modality with respect to CAD diagnosis, treatment and research.

1.10 References

1. "Cardiovascular system" (MedlinePlus, 21-01-2013, 2013), retrieved 03-03-2014, 2014, http://www.nlm.nih.gov/medlineplus/ency/anatomyvideos/000023.htm.
2. M. H. Ross and W. Pawlina, "Cardiovascular System," in Histology, 5 ed. (Lippincott Williams & Wilkins, 2006), p. 364.
3. W. Schaper, "Pathophysiology of coronary circulation," Prog Cardiovasc Dis 14, 275-296 (1971).
4. V. Fuster, R. Walsh, and R. Harrington, Hurst's the Heart, 13th Edition: Two Volume Set (McGraw-Hill Education, 2010).
5. S. M. Grundy, "Cholesterol and coronary heart disease. A new era," JAMA 256, 2849-2858 (1986).
6. I. M. Singh and D. R. Holmes, Jr., "Myocardial revascularization by percutaneous coronary intervention: past, present, and the future," Curr Probl Cardiol 36, 375-401 (2011).
7. W. S. Weintraub, J. A. Spertus, P. Kolm, D. J. Maron, Z. Zhang, C. Jurkovitz, W. Zhang, P. M. Hartigan, C. Lewis, E. Veledar, J. Bowen, S. B. Dunbar, C. Deaton, S. Kaufman, R. A. O'Rourke, R. Goeree, P. G. Barnett, K. K. Teo, W. E. Boden, C. T. R. Group, and G. B. Mancini, "Effect of PCI on quality of life in patients with stable coronary disease," N Engl J Med 359, 677-687 (2008).
8. G. N. Levine, E. R. Bates, J. C. Blankenship, S. R. Bailey, J. A. Bittl, B. Cercek, C. E. Chambers, S. G. Ellis, R. A. Guyton, S. M. Hollenberg, U. N. Khot, R. A. Lange, L. Mauri, R. Mehran, I. D. Moussa, D. Mukherjee, B. K. Nallamothu, H. H. Ting, F. American College of Cardiology, G. American Heart Association Task Force on Practice, A. Society for Cardiovascular, and Interventions, "2011 ACCF/AHA/SCAI Guideline for Percutaneous Coronary Intervention. A report of the American College of Cardiology Foundation/American Heart Association Task Force on Practice Guidelines and the Society for Cardiovascular Angiography and Interventions," J Am Coll Cardiol 58, e44-122 (2011).
9. M. R. Summers and M. R. Patel, "Appropriateness of percutaneous coronary intervention: a review," Curr Cardiol Rep 15, 379 (2013).
10. G. G. Stefanini and D. R. Holmes, Jr., "Drug-eluting coronary-artery stents," N Engl J Med 368, 254-265 (2013).
11. U. Sigwart, J. Puel, V. Mirkovitch, F. Joffre, and L. Kappenberger, "Intravascular stents to prevent occlusion and restenosis after transluminal angioplasty," N Engl J Med 316, 701-706 (1987).
12. T. Kimura, S. Kaburagi, T. Tamura, H. Yokoi, Y. Nakagawa, H. Yokoi, N. Hamasaki, H. Nosaka, M. Nobuyoshi, G. S. Mintz, J. J. Popma, and M. B. Leon, "Remodeling of human coronary arteries undergoing coronary angioplasty or atherectomy," Circulation 96, 475-483 (1997).

13. C. Di Mario, R. Gil, E. Camenzind, Y. Ozaki, C. von Birgelen, V. Umans, P. de Jaegere, P. J. de Feyter, J. R. Roelandt, and P. W. Serruys, "Quantitative assessment with intracoronary ultrasound of the mechanisms of restenosis after percutaneous transluminal coronary angioplasty and directional coronary atherectomy," Am J Cardiol 75, 772-777 (1995).

14. A. E. Rodriguez, O. Santaera, M. Larribau, M. Fernandez, R. Sarmiento, B. Perez, J. B. Newell, G. S. Roubin, and I. F. Palacios, "Coronary stenting decreases restenosis in lesions with early loss in luminal diameter 24 hours after successful PTCA," Circulation 91, 1397-1402 (1995).

15. K. N. Garratt, W. D. Edwards, U. P. Kaufmann, R. E. Vlietstra, and D. R. Holmes, Jr., "Differential histopathology of primary atherosclerotic and restenotic lesions in coronary arteries and saphenous vein bypass grafts: analysis of tissue obtained from 73 patients by directional atherectomy," J Am Coll Cardiol 17, 442-448 (1991).

16. D. L. Fischman, M. B. Leon, D. S. Baim, R. A. Schatz, M. P. Savage, I. Penn, K. Detre, L. Veltri, D. Ricci, M. Nobuyoshi, and et al., "A randomized comparison of coronary-stent placement and balloon angioplasty in the treatment of coronary artery disease. Stent Restenosis Study Investigators," N Engl J Med 331, 496-501 (1994).

17. P. W. Serruys, P. de Jaegere, F. Kiemeneij, C. Macaya, W. Rutsch, G. Heyndrickx, H. Emanuelsson, J. Marco, V. Legrand, P. Materne, and et al., "A comparison of balloon-expandable-stent implantation with balloon angioplasty in patients with coronary artery disease. Benestent Study Group," N Engl J Med 331, 489-495 (1994).

18. D. R. Holmes, Jr., M. Savage, J. M. LaBlanche, L. Grip, P. W. Serruys, P. Fitzgerald, D. Fischman, S. Goldberg, J. A. Brinker, A. M. Zeiher, L. M. Shapiro, J. Willerson, B. R. Davis, J. J. Ferguson, J. Popma, S. B. King, 3rd, A. M. Lincoff, J. E. Tcheng, R. Chan, J. R. Granett, and M. Poland, "Results of Prevention of REStenosis with Tranilast and its Outcomes (PRESTO) trial," Circulation 106, 1243-1250 (2002).

19. P. W. Serruys, M. J. Kutryk, and A. T. Ong, "Coronary-artery stents," N Engl J Med 354, 483-495 (2006).

20. Y. Onuma and P. W. Serruys, "Bioresorbable scaffold: the advent of a new era in percutaneous coronary and peripheral revascularization?," Circulation 123, 779-797 (2011).

21. 2D. Dudek, Y. Onuma, J. A. Ormiston, L. Thuesen, K. Miquel-Hebert, and P. W. Serruys, "Four-year clinical follow-up of the ABSORB everolimus-eluting bioresorbable vascular scaffold in patients with de novo coronary artery disease: the ABSORB trial," EuroIntervention 7, 1060-1061 (2012).

22. J. Tanigawa, P. Barlis, K. Dimopoulos, M. Dalby, P. Moore, and C. Di Mario, "The influence of strut thickness and cell design on immediate apposition of drug-eluting stents assessed by optical coherence tomography," Int J Cardiol 134, 180-188 (2009).

23. J. H. Reiber, "Introduction to QCA, IVUS and OCT in interventional cardiology," Int J Cardiovasc Imaging 27, 153-154 (2011).

24. R. Hamdan, R. G. Gonzalez, S. Ghostine, and C. Caussin, "Optical coherence tomography: from physical principles to clinical applications," Arch Cardiovasc Dis 105, 529-534 (2012).

25. H. G. Bezerra, M. A. Costa, G. Guagliumi, A. M. Rollins, and D. I. Simon, "Intracoronary optical coherence tomography: a comprehensive review clinical and research applications," JACC Cardiovasc Interv 2, 1035-1046 (2009).

26. S. Tahara, H. G. Bezerra, M. Baibars, H. Kyono, W. Wang, S. Pokras, E. Mehanna, C. L. Petersen, and M. A. Costa, "In vitro validation of new Fourier-domain optical coherence tomography," EuroIntervention 6, 875-882 (2011).

27. F. Abtahian and I. K. Jang, "Optical coherence tomography: basics, current application and future potential," Curr Opin Pharmacol 12, 583-591 (2012).

28. S. Elahi, M. D. Feldman, J. Dijkstra, and T. E. Milner, "Intravascular optical coherence tomography measurement of size and apposition of metallic stents," Biomed Opt Express 4, 1876-1882 (2013).

29. S. Elahi, J. J. Mancuso, T. E. Milner, and M. D. Feldman, "Sunflower artifact in OCT," JACC Cardiovasc Imaging 4, 1220-1221 (2011).

30. K. Levitt, L. Vivas, B. Courtney, and K. A. Connelly, "Vascular imaging in diabetes," Curr Atheroscler Rep 16, 399 (2014).

31. A. V. Finn, Y. Chandrashekhar, and J. Narula, "IVUS and OCT: either or survivor," JACC Cardiovasc Imaging 4, 1047-1049 (2011).

32. T. Kubo, A. Tanaka, H. Kitabata, Y. Ino, T. Tanimoto, and T. Akasaka, "Application of optical coherence tomography in percutaneous coronary intervention," Circ J 76, 2076-2083 (2012).

33. S. Tsantis, G. C. Kagadis, K. Katsanos, D. Karnabatidis, G. Bourantas, and G. C. Nikiforidis, "Automatic vessel lumen segmentation and stent strut detection in intravascular optical coherence tomography," Med Phys 39, 503-513 (2012).

34. L. Hebsgaard, E. H. Christiansen, and N. R. Holm, "Calibration of intravascular optical coherence tomography as presented in peer reviewed publications," Int J Cardiol 171, 92-93 (2014).

35. S. Gurmeric, G. G. Isguder, S. Carlier, and G. Unal, "A new 3-D automated computational method to evaluate in-stent neointimal hyperplasia in in-vivo intravascular optical coherence tomography pullbacks," Med Image Comput Comput Assist Interv 12, 776-785 (2009).

36. A. Wang, J. Eggermont, N. Dekker, H. M. Garcia-Garcia, R. Pawar, J. H. C. Reiber, and J. Dijkstra, "A robust automated method to detect stent struts in 3D intravascular optical coherence tomographic image sequences," in Medical Imaging, 2012), 83150L-83150L-83159.

37. G. Unal, S. Gurmeric, and S. G. Carlier, "Stent implant follow-up in intravascular optical coherence tomography images," Int J Cardiovasc Imaging 26, 809-816 (2010).

38. G. J. Ughi, T. Adriaenssens, W. Desmet, and J. D'Hooge, "Fully automatic three-dimensional visualization of intravascular optical coherence tomography images: methods and feasibility in vivo," Biomed Opt Express 3, 3291-3303 (2012).

39. G. J. Ughi, T. Adriaenssens, K. Onsea, P. Kayaert, C. Dubois, P. Sinnaeve, M. Coosemans, W. Desmet, and J. D'Hooge, "Automatic segmentation of in-vivo intra-coronary optical coherence tomography images to assess stent strut apposition and coverage," Int J Cardiovasc Imaging 28, 229-241 (2012).

40. F. Nakao, T. Ueda, S. Nishimura, H. Uchinoumi, M. Kanemoto, N. Tanaka, and T. Fujii, "Guide wire shadow assessed by shading index is reduced in sparse spring coil wire in optical coherence tomography," Cardiovasc Interv Ther 28, 362-367 (2013).

41. A. Wang, J. Eggermont, J. H. C. Reiber, N. Dekker, P. J. H. de Koning, and J. Dijkstra, "Assessment of implanted stent coverage of side-branches in intravascular optical coherence tomographic images," in Medical Imaging, 2013), 86703J-86703J-86708.

42. K. Mandelias, S. Tsantis, D. Karnabatidis, P. Katsakiori, D. Mihailidis, G. Nikiforidis, and G. C. Kagadis, "Fast and Robust Algorithm Towards Vessel Lumen and Stent Strut Detection in Optical Coherence Tomography," Med.Phys. 39, 3645-3646 (2012).

43. H. Takebayashi, G. S. Mintz, S. G. Carlier, Y. Kobayashi, K. Fujii, T. Yasuda, R. A. Costa, I. Moussa, G. D. Dangas, R. Mehran, A. J. Lansky, E. Kreps, M. B. Collins, A. Colombo, G. W. Stone, M. B. Leon, and J. W. Moses, "Nonuniform strut distribution correlates with more neointimal hyperplasia after sirolimus-eluting stent implantation," Circulation 110, 3430-3434 (2004).

44. Y. Suzuki, F. Ikeno, and A. Yeung, "Drug-Eluting Stents strut distribution; A comparison of 3 stent designs by optical coherence tomography," Am J Cardiol 96, 182H-182H (2005).

45. M. P. Opolski, R. Pracon, G. S. Mintz, T. Okabe, J. Pregowski, S. Y. Lee, E. C. van der Waal, L. Kalinczuk, P. Roy, K. A. Smith, R. Torguson, Z. Xue, L. F. Satler, K. M. Kent, A. D. Pichard, R. Waksman, and N. J. Weissman, "Relation of drug-eluting stent strut distribution to stent thrombosis in coronary arteries," Am J Cardiol 104, 343-348 (2009).

46. Y. Suzuki, F. Ikeno, and A. C. Yeung, "Drug-eluting stent strut distribution: a comparison between Cypher and Taxus by optical coherence tomography," J Invasive Cardiol 18, 111-114 (2006).

47. S. Tanimoto, N. Bruining, D. Rotger, P. Radeva, J. M. Ligthart, R. T. van Domburg, and P. W. Serruys, "Late stent recoil of the bioabsorbable everolimus fluting coronary stent and its relationship with stent strut distribution and plaque morphology," Am J Cardiol 100, 145L-145L (2007).

48. M. P. Opolski, R. Pracon, G. S. Mintz, N. J. Weissman, L. Mandinov, J. Pregowski, M. Kruk, A. Witkowski, H. Wang, S. G. Ellis, E. Grube, K. D. Dawkins, and G. W. Stone, "Stent Strut Distribution at Implantation and 9-Month Follow-up in TAXUS and Bare Metal Stents and Its Effect on Neointimal Hyperplasia. An Intravascular Ultrasound Integrated Analysis of the Randomized TAXUS IV, V and VI Trials," Journal of the American College of Cardiology 53, A9-A9 (2009).

49. A. Wang, J. Eggermont, N. Dekker, J. H. Reiber, and J. Dijkstra, "Semi-automatic Measurement of Vessel Wall Support from I mplanted Stents in I VOCT I mage Sequences," in MICCAI 2013 STENT, 2013),

50. J. L. Gutierrez-Chico, M. D. Radu, R. Diletti, A. Sheehy, M. B. Kossuth, J. P. Oberhauser, T. Glauser, J. Harrington, R. J. Rapoza, Y. Onuma, and P. W. Serruys, "Spatial distribution and temporal evolution of scattering centers by optical coherence tomography in the poly(L-lactide) backbone of a bioresorbable vascular scaffold," Circ J 76, 342-350 (2012).

51. A. Sheehy, J. L. Gutierrez-Chico, R. Diletti, J. P. Oberhauser, T. Glauser, J. Harrington, M. B. Kossuth, R. J. Rapoza, Y. Onuma, and P. W. Serruys, "In vivo characterisation of bioresorbable vascular scaffold strut interfaces using optical coherence tomography with Gaussian line spread function analysis," Eurointervention 7, 1227-1235 (2012).

52. A. Wang, J. Eggermont, N. Dekker, P. J. de Koning, J. H. Reiber, and J. Dijkstra, "3D assessment of stent cell size and side branch access in intravascular optical coherence tomographic pullback runs," Comput Med Imaging Graph 38, 113-122 (2014).

53. P. Mortier, M. De Beule, D. Van Loo, B. Verhegghe, and P. Verdonck, "Finite element analysis of side branch access during bifurcation stenting," Med Eng Phys 31, 434-440 (2009).

54. B. Hong, K. Z. Wang, Q. H. Huang, Y. Xu, X. G. Fang, Z. Li, and J. M. Liu, "Effects of metal coverage rate of flow diversion device on neointimal growth at side branch ostium and stented artery: an animal experiment in rabbit abdominal aorta," Neuroradiology 54, 849-855 (2012).

55. 55. F. Burzotta, M. De Vita, G. Sgueglia, D. Todaro, and C. Trani, "How to solve difficult side branch access?," Eurointervention 6, J72-J80 (2010).

56. 56. I. K. Jang, "Optical coherence tomography or intravascular ultrasound?," JACC Cardiovasc Interv 4, 492-494 (2011).

57. A. Wang, J. Eggermont, N. Dekker, H. M. Garcia-Garcia, R. Pawar, J. H. Reiber, and J. Dijkstra, "Automatic stent strut detection in intravascular optical coherence tomographic pullback runs," Int J Cardiovasc Imaging 29, 29-38 (2013).

58. A. Wang, S. Nakatani, J. Eggermont, Y. Onuma, H. M. Garcia-Garcia, P. W. Serruys, J. H. C. Reiber, and J. Dijkstra, "Automatic detection of bioresorbable vascular scaffold struts in intravascular optical coherence tomography pullback runs," Biomed Opt Express 5, 3589-3602 (2014).

59. A. Wang, J. Eggermont, J. H. C. Reiber, and J. Dijkstra, "Fully automated side branch detection in intravascular optical coherence tomography pullback runs," Biomed Opt Express 5, 3160-3173 (2014).